Tethers as Debris: Simulating Impacts of Tether Fragments on Shuttle Tiles

Steven W. Evans*
NASA Marshall Space Flight Center, Huntsville, Alabama,35812

The SPHC hydrodynamic code was used to simulate impacts of Kevlar™ and aluminum projectiles on a model of the LI-900 type insulating tiles used on Space Shuttle Orbiters. The intent was to examine likely damage that such tiles might experience if impacted by orbital debris consisting of tether fragments. Projectile speeds ranged from 300 m/s to 10 km/s. Damage is characterized by penetration depth, tile surface-hole diameter, tile body-cavity diameter, coating fracture diameter, tether and cavity wall material phases, and deformation of the aluminum backwall.

I. Introduction

A companion paper[1] in this session gave a description of the SPHC hydrodynamic code, and described its results when applied to the problem of spherical aluminum projectiles striking single-wall and double-wall aluminum shields. For this paper SPHC was used to examine the probable results of impacts of tether fragments on thermal insulating tiles such as those on the Space Shuttle Orbiters. Tethers are subject to sever by impacts of orbital debris and meteoroids. Consequently they may produce tether fragments that, despite their short orbital lifetimes, could collide with a Shuttle on orbit. This is true of tethers being used to deploy satellites from a Shuttle payload bay. In such a case a tether fragment could recontact the Shuttle, perhaps after a few orbits, and, owing to the differential drag between the tether and Shuttle, the recontact speed could amount to a few hundred meters per second. An alternative case would be the presence of a tether in orbit from a mission totally unrelated to a Shuttle flight that nevertheless impacts the Shuttle – collision avoidance might be impossible if the tether is not trackable by ground observers or radars. In such a case the impact speed depends on the inclination difference between the orbits of the Shuttle and the tether fragment. Damage to tiles resulting from such impacts is seen to range from narrow channels for the slow impacts, to almost total destruction of tiles and penetrating cracks and spall of their aluminum substrate walls for the fast impacts.

II. Simulations

The following section outlines the simulations performed and the results obtained.

A. Physical Elements

The tether fragments were modeled as bundles of seven 1-mm strands, with the bundles having diameters of 3 mm. In the three dimensional simulation the bundle length was 20 cm. The tethers were of either Kevlar™49 or aluminum 6061-T6. These represent non-conducting and conducting tethers, respectively, types which have been contemplated for various tether missions. Tethers were modeled using a Mie-Gruneisen analytic equation of state (eos), including phase changes from solid to liquid, vapor, and plasma.

The tile model was developed during the STS-107 accident investigation.[2] The tile was 6-in square, and included several layers making up its structure. The outermost layer was a relatively dense "reaction cured glass" (RCG), 0.5-mm thick, which was present on the top and sides of the tile. Below this coating was the bulk of the tile, 1.8-in thick, made of a rigidized fibrous silica product known as LI-900, with a density of 9 lb/ft^3. Below this main insulating layer was a bottom layer of LI-900 that was treated to increase its density by approximately 69% to improve its strength. The densified layer was bonded to a Strain Isolation Pad (SIP), modeled as a refractory felt fabric. The SIP was in turn bonded to an aluminum 2024 wall 0.1-in thick. The tile and backwall materials used a Mie-Gruneisen

* Aerospace Engineer, Environments Group, Mail Stop ED44, Member AIAA.

multiphase eos, with the exception of the SIP felt, which used a "fabric" equation of state. Fabrics must crush to the full bulk material density before the bulk properties and a Mie-Gruneisen eos are applied.

Material properties required in the simulations were obtained from internal NASA sources and from the *MatWeb.com* website: http://www.matweb.com/ during the STS-107 investigation in 2003.

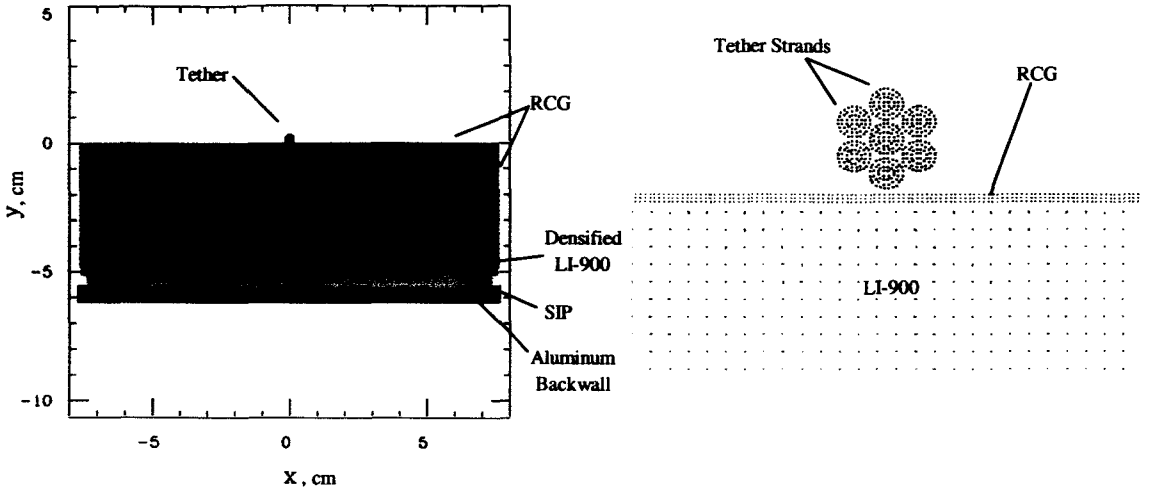

Figure 1: a. Overall tether-on-tile setup. b. Detail of tether strands and top of tile.

B. Simulation List

Situations in which a tether – Shuttle encounter might occur include a sever accident during a deployment, and collision by a tether fragment unrelated to any Shuttle activity. In a sever accident the encounter could occur after one or a few orbits, assuming the Shuttle performed no collision avoidance maneuver. The relative velocity would be only a few hundred meters per second, due almost entirely to the differential drag between the tether fragment and the Shuttle. Cases of this type are represented by impact simulations at 300 m/s. Encounters with unrelated tether fragments could cover the entire speed range to be expected from objects making up the orbital debris environment. Assuming circular orbits at a typical Shuttle altitude of 400km, the encounter speeds for the orbital inclination differences specified in Table 1 would be produced. In this table the approach azimuth is the angular direction in the local horizontal plane off the Shuttle velocity vector from which the tether fragment would appear.

Two dimensional simulations were performed at each of the speeds in Table 1, with memory reserved for 20,000 SPH particles at the first three speeds, and memory for 80,000 particles reserved for the 10 km/s cases. This added memory allowed greater resolution of the events occuring at this high speed. In addition, a three dimensional simulation was performed at 7 km/s to compare the results for aluminum tethers in the 2-D and 3-D cases. Memory was reserved for 240,000 SPH particles for this run. The full simulation list is noted in Table 2.

Table 1: Encounter Speeds vs. Orbital Inclination Difference

Δi deg	V km/s	Approach Azimuth deg
2.2	0.3	88.9
22.6	3.0	78.7
54.3	7.0	62.8
81.4	10.0	49.3

Table 2: Run List – Impact Velocities Normal to Tile Surface
Tether Axis Parallel to Tile Surface

	Number of Particles		
	2-D Runs		3-D Run
V, km/s	Kevlar	Aluminum	Aluminum
0.3	20,000	20,000	
3.0	20,000	20,000	
7.0	20,000	20,000	240,000
10.0	80,000	80,000	

C. Comparison of 2-D and 3-D Simulations

Figure 2 shows the 3-D simulation setup. Figure 3 compares the 2-D simulation with a cross-section through the 3-D simulation both at setup and at 10 μs into the runs. Note the relative coarseness of the 3-D sim despite the large number of particles allocated to this setup. The huge number of particles required to achieve comparable fineness of zoning of 3-D cases relative to 2-D cases is a problem because run times are severely lengthened. If comparable results can be realized, then using 2-D sims is definitely to be preferred. At 10 μs the 2-D sim cavity is 3.0 cm in diameter, whereas the 3-D sim cavity is ~3.8 cm, though this measurement is uncertain due to the burst of particles

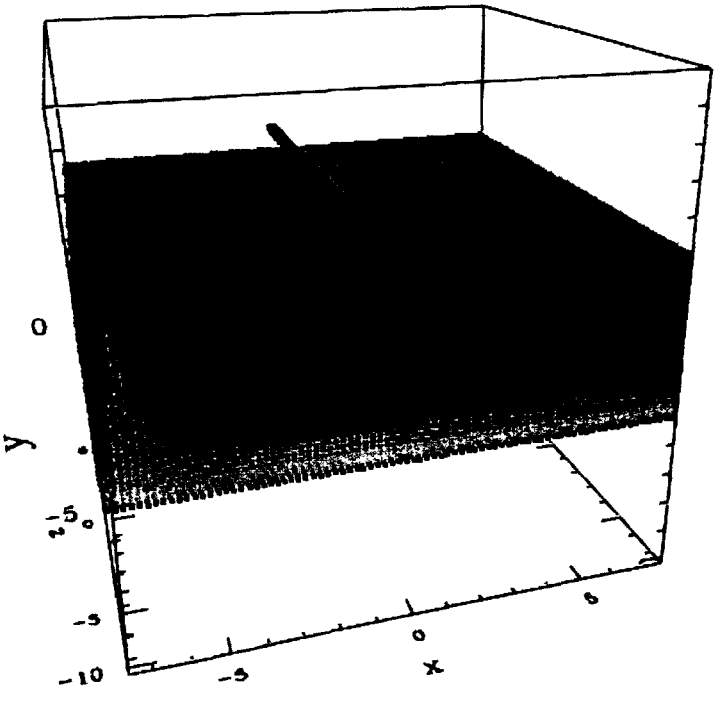

Figure 2: 3-D setup for aluminum tether on tile at 7 km/s.

into the cavity. Cavity shapes are similar, but the tether debris penetrates much deeper in the 3-D case. This illustrates a problem seen when the zoning is coarse – particles from the impactor tend to slip through the spaces in the tile matrix, traveling farther than one would expect in reality. The comparison shows that the results do differ somewhat, but they are similar enough that the remaining cases were run in two dimensions, to save computation time and avoid the zoning and unrealistic travel problems.

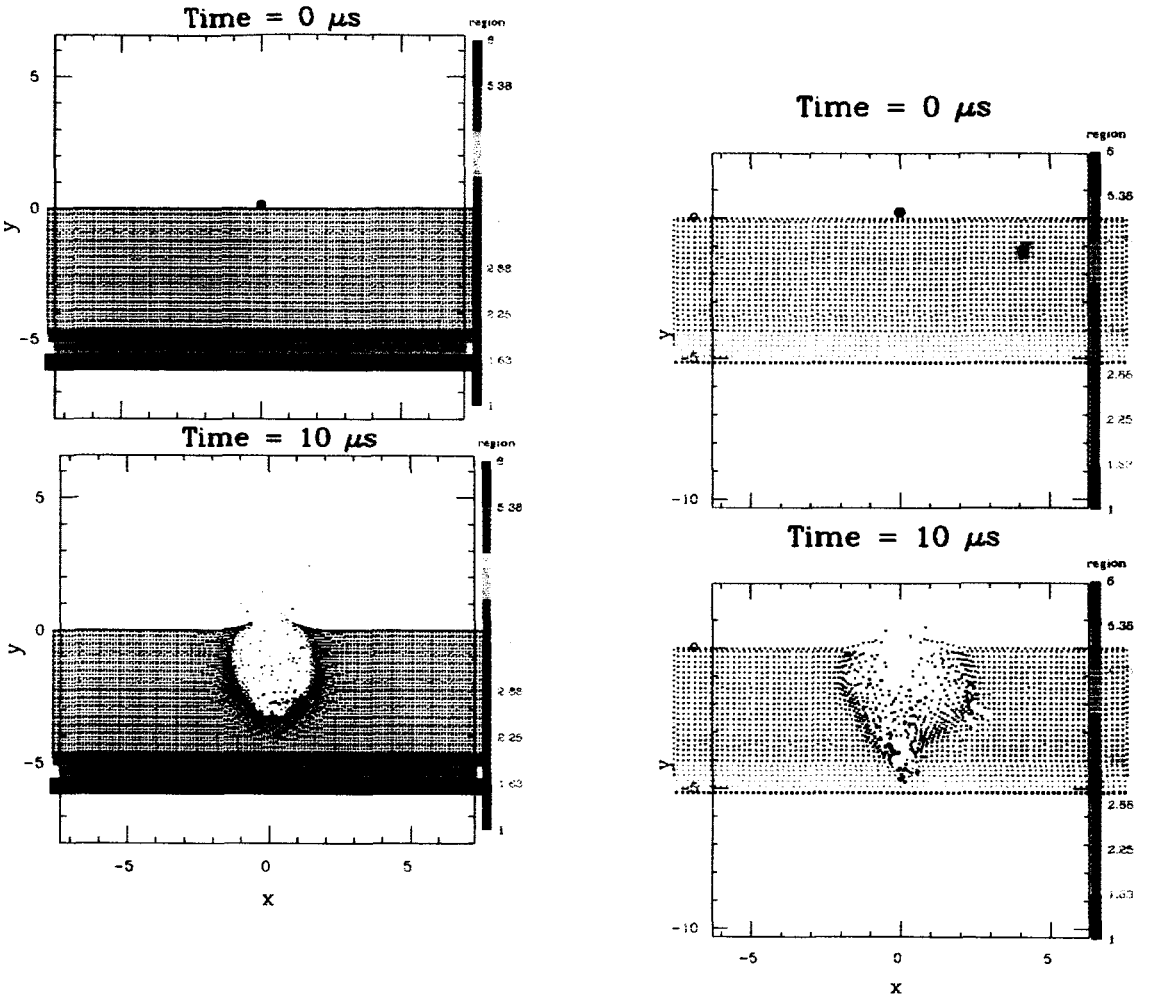

Figure 3: Aluminum tether on tile: left, 2-D simulation; right, section through 3-D simulation.

D. Damage Descriptions

Damage to the tiles was characterized according to tether material by hole diameter in the upper surface, diameter of the cavity excavated along the length of the impacting tether, depth of the cavity, and width of the strip of RCG fractured off the surface. All measurements concluded at the 100 μs point; motion had not totally ceased at this point, especially in the high-speed cases, so final damage is expected to be more extensive. Damage for each tether type and speed is given in Tables A1 to A8 in the Appendix.

1) Low-speed impacts: 300 m/s. Neither Kevlar nor aluminum tethers produced severe damage in the low-speed impacts. The tethers cut a channel into the tile surface, less than 2 cm deep. The aluminum held together better than the Kevlar, so its damage channel was not as wide and was slightly deeper. Blades of fracture radiated from the channel ~1 cm downward and to either side, failing to travel the full thickness of the LI-900. No damage was observed to the densified LI-900 layer, the SIP, or the backwall. A shell of RCG ~4 cm across fractured away from the point of impact. There was no melting of any component. The impact energy was dissipated primarily in deformation of the tether and of the main body of the LI-900. See Fig. 4. Damage of this severity should not compromise a Shuttle reentry unless it occurred at an especially vulnerable location.

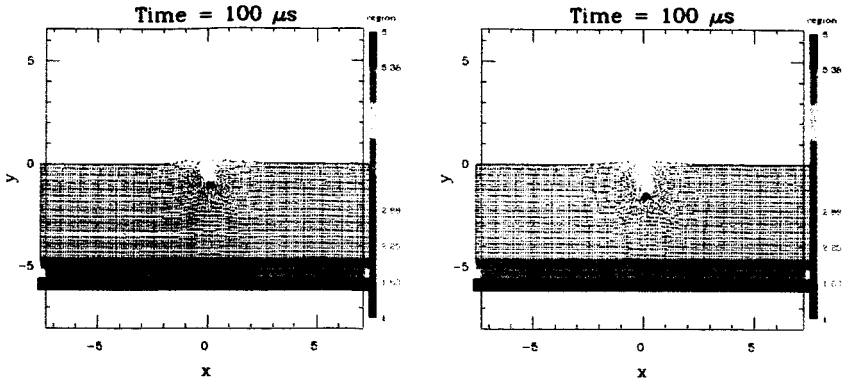

Figure 4: Impacts at 300 m/s: left - Kevlar; right- aluminum.

2) Low-hypervelocity: 3 km/s. The Kevlar was smashed, melted, and pooled in the bottom of the cavity, with minor production of Kevlar vapor. A cavity of roughly egg-shaped cross section was formed. Its walls were fractured in a broad prism centered on the point of impact, with small boundary cracks opening at about a third of the depth. The fracture zone extended through the full thickness of the LI-900; the densified layer was fractured down to the SIP and compressed to a 2-mm thickness from an original 5 mm; the SIP was compressed from 4 mm down to 2 mm. There was no backwall deformation. The whole top RCG layer appeared to disintegrate. The cental panel of Fig. 5 shows the scene plotted on phase: dark blue material is fractured, aqua shows plastic deformation, yellow is liquid, and red is vapor.

The aluminum impact created a cavity more spindle-shaped in cross section, owing to the greater penetration of the denser aluminum into the tile. Damage to the tile was similar to the Kevlar case, but with more compression of the densified layer (to 1 mm) and the SIP, which was crushed out of view. Here the backwall suffered a deflection of ~1mm. Again the RCG layer disintegrated.

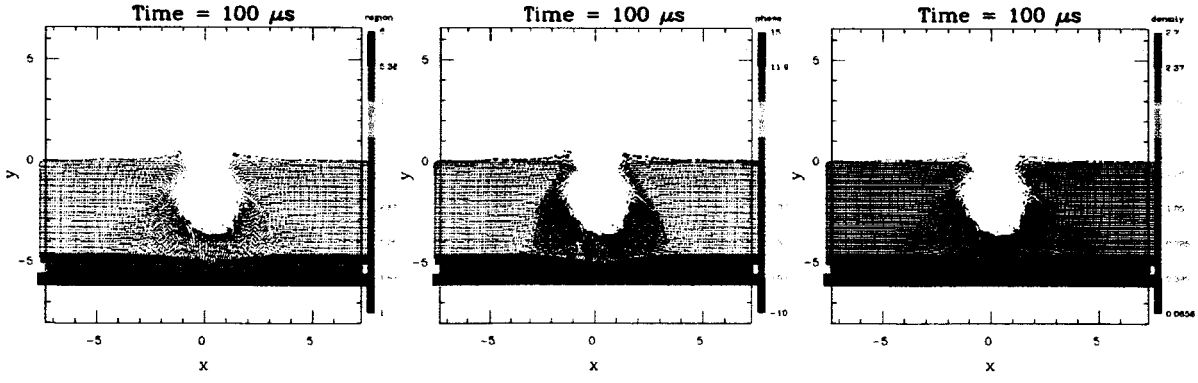

Figure 5: Kevlar at 3 km/s: left, by region; center, by phase; right, by density.

3) Mid-hypervelocity: 7 km/s. Here explosive cavity formation is observed, with the Kevlar melting and vaporizing. The cavity begins with a circular cross section but develops into a vertical-walled, wedge-bottomed shape at late times. Its walls are completely fractured. The densified LI-900 is crushed to ~1 mm thickness, and the SIP is crushed out of view. It appears the crushing of these two bottom layers will produce a roughly flat-bottomed cavity. Despite the extensive destruction of the tile, most of which will probably disintegrate, the backwall is only slightly deformed. See Fig. 6.

The explosive release of impact energy is carried deeper into the tile by the denser aluminum, resulting in a cavity wider near its base than at the top. The cavity walls are fractured, with fracture progressing below the RCG to LI-900 interface and along the LI-900 to densified LI-900 interface. The tether liquifies, and there is LI-900 vapor present in the cavity. For aluminum at 7 km/s the first indication of serious backwall damage is seen. The backwall deflects ~5 mm, and there is a fractured zone below the pool of tether material. It appears a plug ~1.4 cm across might detach at later times. This is the first indication that a structural or pressure-integrity failure might result from a tether impact. See Fig. 7.

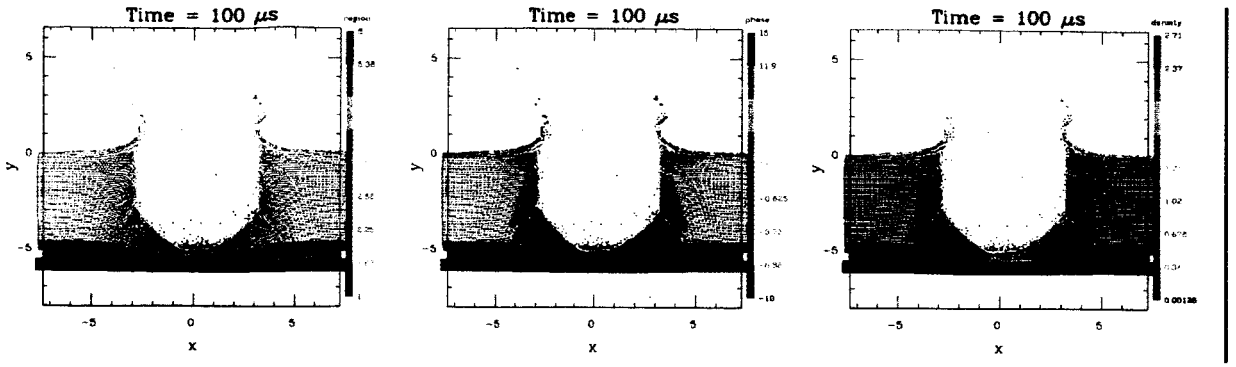

Figure 6: Kevlar at 7 km/s: left, by region; center, by phase; right, by density.

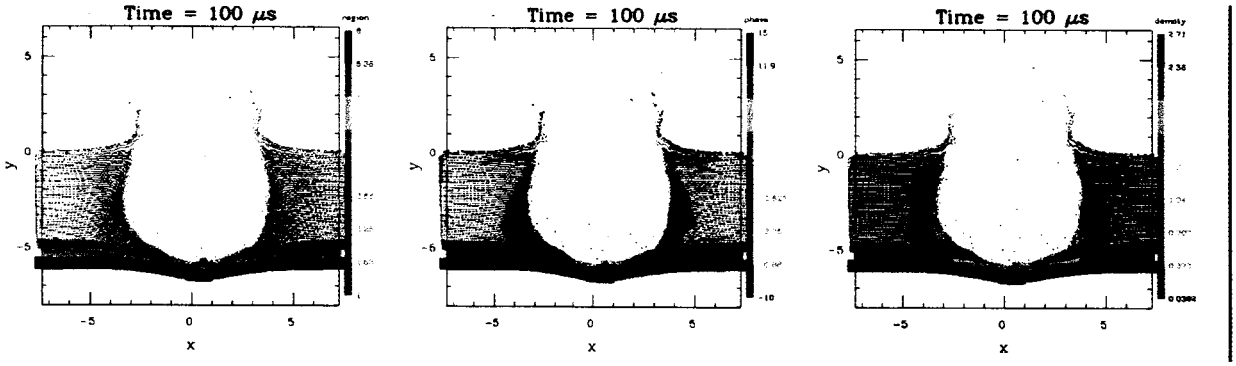

Figure 7: Aluminum at 7 km/s: left, by region; center, by phase; right, by density.

4) Hypervelocity: 10 km/s. At this extreme speed the Kevlar tether has almost totally vaporized. The excess of the impact energy beyond that needed to accomplish this phase change has been dissipated in explosively accelerating the mass of the LI-900 tile material, producing a huge, rapidly-expanding cavity that would ultimately sweep away the entire tile. What remains of the LI-900, densified layer, and SIP directly under the impact point has been crushed to a thickness of ~3 mm. Interestingly, the damage to the aluminum backwall is modest, amounting to a broad deflection of ~1 to 2 mm, without any fracture or perforation. See Fig. 8.

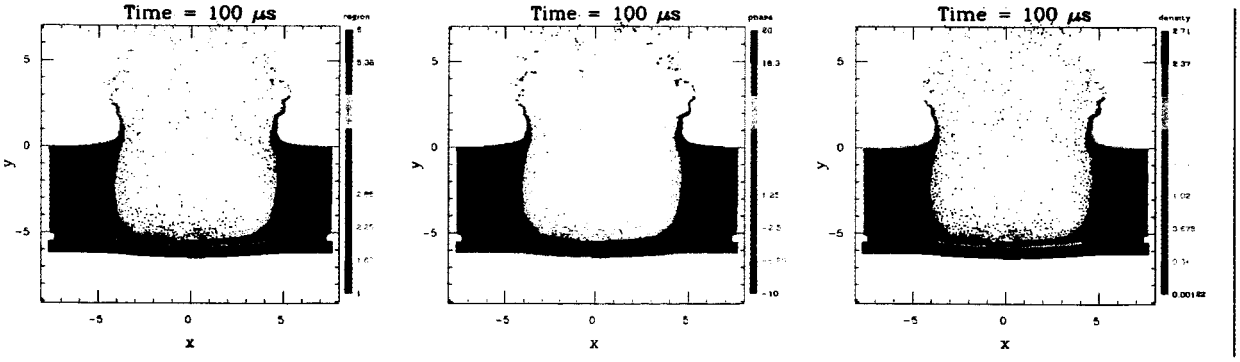

Figure 8: Kevlar at 10 km/s: left, by region; center, by phase; right, by density.

The aluminum at 10 km/s imparts similar damage to the tile, but penetrates further, ending up as a pool of liquid against the crushed and delaminating material over the backwall. The backwall itself now sustains wave-like plastic deformation of its surface, deflection by ~1.7 cm, an opening crack below the center of impact, and a hinging shear crack ~2.8 cm to the right. This is sufficient damage to destroy any thermal value of the tile, and compromise the pressure integrity, and, possibly, the structural integrity, of the backwall. See Fig. 9.

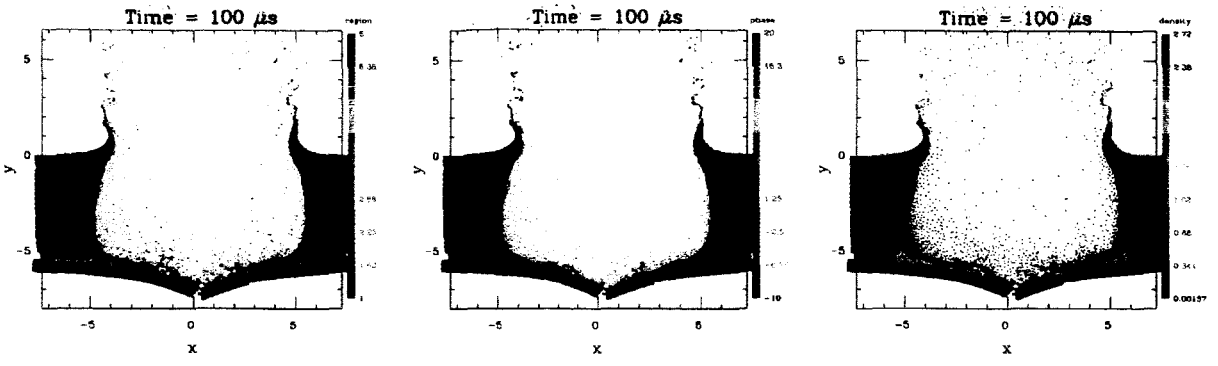

Figure 9 : Aluminum at 10 km/s: left, by region; center, by phase; right, by density.

III. Conclusion

This series of impact simulations has shown that at 300 m/s, impacts by small tethers on Shuttle tiles will produce minimal damage, amounting to the cutting of channels into the tiles of a breadth comparable to, and depth 4 to 5 times that of the tether itself. Unless the tether is much larger or the tile is much thinner than the 1.8-in LI-900 tile simulated here, there should not be exposure of the aluminum backwall, and consequent serious thermal risk during reentry. Even at 3 km/s, the damage to the tile was modest, and might not pose a reentry risk. Thus tether fragments from sever accidents during deployment from a Shuttle, and independent tether fragments in orbits with small inclination differences to the Shuttle orbit would not be serious flight risks, provided they are small diameter objects. Tethers with orbits of higher inclination difference, say, above 50 deg, do pose a significant damage risk to the Shuttle, as shown by the 7 km/s and 10 km/s impact results presented here. Damage to structural walls behind the tiles commences in this speed range if the tether is of the multi-strand metal conductor type. Non-conducting polymer tethers may not perforate a structural wall, but would remove large areas of tile, possibly compromising the thermal integrity of the surface during reentry.

Appendix

Table A1: Damage by Kevlar at 300 m/s

Time μs	Hole Diam cm	Cavity Diam cm	Cavity Depth cm	RCG Fracture cm
5	0.3	0.3	0.1	
10	0.3	0.3	0.2	
15	0.4	0.4	0.3	
20	0.5	0.5	0.4	
25	0.5	0.5	0.5	
30	0.5	0.5	0.6	
35	0.5	0.5	0.6	1.7
40	0.5	0.5	0.6	
45	0.6	0.6	0.6	2.0
50	0.6	0.7	0.7	
55	0.6	0.7	0.7	2.5
60		0.8	0.8	2.6
65		0.8	0.8	2.7
70		0.8	0.8	2.9
75		0.8	0.9	3.5
80		0.9	0.9	3.7
85		1.0	1.0	3.7
90		1.0	1.0	4.0
95		1.0	1.0	4.2
100		1.0	1.1	4.4

Table A2: Damage by Aluminum at 300 m/s

Time μs	Hole Diam cm	Cavity Diam cm	Cavity Depth cm	RCG Fracture cm
5	0.3	0.3	0.1	
10	0.3	0.3	0.2	
15	0.3	0.3	0.3	
20	0.4	0.4	0.4	0.7
25	0.4	0.4	0.5	1.1
30	0.5	0.4	0.6	1.4
35	0.5	0.4	0.6	1.6
40	0.5	0.5	0.7	1.8
45	0.5	0.5	0.8	2.0
50	0.5	0.5	0.9	2.3
55	0.6	0.5	1.0	2.6
60	0.6	0.6	1.0	2.9
65	0.6	0.6	1.1	3.0
70	0.7	0.6	1.1	3.1
75	0.7	0.6	1.2	3.3
80	0.7	0.6	1.2	3.5
85	0.7	0.6	1.2	4.0
90		0.6	1.3	4.2
95			1.4	4.5
100			1.5	4.6

Table A3: Damage by Kevlar at 3 km/s

Time μs	Hole Diam cm	Cavity Diam cm	Cavity Depth cm	RCG Fracture cm
5	0.6	0.8	0.9	
10	0.8	1.3	1.3	1.3
15	0.9	1.5	1.6	1.8
20	1.1	1.8	2.0	2.5
25	1.1	1.9	2.1	3.0
30	1.2	2.2	2.3	4.0
35	1.4	2.4	2.5	4.1
40	1.4	2.5	2.6	4.5
45	1.6	2.7	2.7	4.9
50	1.6	2.7	2.9	5.0
55	1.7	2.9	3.0	5.4
60	1.7	3.0	3.0	5.7
65	1.8	3.1	3.1	6.1
70	1.9	3.2	3.1	6.4
75	2.0	3.3	3.3	6.6
80	2.0	3.4	3.4	10.3
85	2.2	3.4	3.4	11.8
90	2.3	3.4	3.4	12.0
95	2.3	3.6	3.6	14.4
100	2.3	3.6	3.7	14.6

Table A4: Damage by Aluminum at 3 km/s

Time μs	Hole Diam cm	Cavity Diam cm	Cavity Depth cm	RCG Fracture cm
5	0.6	0.9	1.0	0.8
10	0.9	1.3	1.8	1.3
15	1.0	1.7	2.3	2.0
20	1.1	2.0	2.7	2.6
25	1.3	2.2	3.1	3.3
30	1.4	2.3	3.4	3.6
35	1.5	2.5	3.6	5.0
40	1.6	2.5	3.9	5.4
45	1.6	2.7	4.1	5.7
50	1.7	2.9	4.3	6.1
55	1.8	3.0	4.4	6.2
60	1.9	3.2	4.5	6.6
65	2.0	3.3	4.6	7.3
70	2.1	3.3	4.7	11.0
75	2.1	3.4	4.8	11.5
80		3.5	4.9	11.9
85		3.6	4.9	11.9
90		3.6	5.0	12.0
95		3.8	5.0	12.2
100		4.0	5.1	12.4

Table A5: Damage by Kevlar at 7 km/s

Time μs	Hole Diam cm	Cavity Diam cm	Cavity Depth cm	RCG Fracture cm
5	1.0	2.1	1.8	2.2
10	1.3	2.8	2.3	3.5
15	1.6	3.2	2.8	4.4
20	1.8	3.6	3.0	5.5
25	2.1	3.9	3.3	6.0
30	3.3	4.2	3.5	6.6
35	3.5	4.4	3.8	7.3
40	3.7	4.6	4.0	8.4
45	3.9	4.7	4.1	8.8
50	4.2	4.9	4.2	9.1
55	4.3	5.1	4.3	9.5
60	4.8	5.3	4.4	10.6
65	4.8	5.4	4.6	11.3
70	5.0	5.5	4.6	13.0
75	5.4	5.6	4.6	13.3
80	5.6	5.8	4.7	13.6
85	5.9	5.9	4.7	13.7
90	6.0	6.1	4.8	14.0
95		6.2	4.8	14.2
100		6.3	4.8	14.3

Table A6: Damage by Aluminum at 7 km/s

Time μs	Hole Diam cm	Cavity Diam cm	Cavity Depth cm	RCG Fracture cm
5	0.8	2.2	2.0	2.3
10	1.4	3.0	3.1	3.6
15	1.7	3.3	4.0	4.5
20	1.9	3.9	4.5	5.5
25	2.2	4.3	4.9	6.4
30	2.5	4.6	5.1	7.1
35	2.7	4.9	5.1	7.6
40	2.9	5.2	5.1	8.2
45	3.2	5.4	5.2	9.3
50	3.4	5.6	5.2	9.8
55	3.7	5.8	5.3	10.3
60	3.8	6.1	5.3	10.7
65	4.0	6.2	5.3	13.0
70	4.6	6.4	5.3	15.2
75	4.8	6.6	5.4	
80	5.0	6.7	5.4	
85	5.3	6.9	5.6	
90	5.3	7.0	5.6	
95	5.6	7.2	5.6	
100	5.7	7.4	5.6	

Table A7: Damage by Kevlar at 10 km/s

Time μs	Hole Diam cm	Cavity Diam cm	Cavity Depth cm	RCG Fracture cm
5	0.5	2.2	2.1	2.9
10	0.8	3.7	3.1	4.6
15	1.0	4.4	3.7	5.8
20	1.3	4.9	4.0	6.8
25	2.7	5.6	4.4	7.6
30	3.9	6.0	4.6	8.6
35	4.2	6.3	4.9	9.1
40	4.8	6.7	5.0	9.8
45	5.3	7.0	5.2	10.3
50	5.8	7.2	5.2	11.1
55	6.6	7.4	5.2	11.6
60	6.7	7.8	5.2	12.0
65	6.7	8.0	5.2	12.3
70	7.0	8.1	5.2	12.8
75	7.2	8.3	5.3	13.1
80	7.5	8.5	5.3	13.7
85	7.7	8.8	5.4	14.0
90	7.9	9.0	5.4	14.9
95	8.1	9.2	5.4	15.1
100	8.3	9.3	5.4	15.2

Table A8: Damage by Aluminum at 10 km/s

Time μs	Hole Diam cm	Cavity Diam cm	Cavity Depth cm	RCG Fracture cm
5	0.5	2.5	2.9	2.9
10	0.8	3.7	4.3	4.3
15	2.0	4.6	5.0	5.2
20	2.5	5.2	5.2	6.2
25	3.5	5.8	5.4	7.0
30	3.8	6.4	5.5	8.3
35	4.3	6.8	5.6	8.9
40	4.6	7.2	5.7	9.3
45	4.9	7.5	5.7	9.8
50	5.3	7.9	5.8	10.4
55	5.6	8.2	5.9	10.9
60	5.9	8.6	6.0	11.3
65	6.2	8.8	6.1	11.7
70	7.0	9.0	6.1	12.2
75	7.5	9.3	6.2	12.6
80	7.7	9.5	6.3	13.0
85	7.9	9.8	6.4	13.4
90	8.2	10.0	6.4	13.9
95	8.3	10.2	6.6	14.2
100	8.5	10.4	6.7	14.2

Acknowledgments

The author thanks Dr. Robert F. Stellingwerf for extensive consultations and assistance in setting up the input files and running the SPHC code during the course of this study.

References

[1]Evans, S. W., Stallworth, R., and Stellingwerf, R. F., "Comparison of SPHC Hydrocode Results with Penetration Equations and Results of Other Codes," *45th AIAA/ASME/ASCE/AHS Structures, Structural Dynamics, and Materials Conference*, Palm Springs, CA, April 2004.

[2]Stellingwerf, R. F., Robinson, J. H., Richardson, S., Evans, S. W., Stallworth, R., and Hovater, M., "Foam-on-Tile Impact Modeling for the STS-107 Investigation," *42nd AIAA Aerospace Sciences Meeting and Exhibit*, Reno, NV, January 2004.